

Observation of the Onset of Constituent Quark Number Scaling in Heavy-Ion Collisions at RHIC

The STAR Collaboration
(Dated: April 4, 2025)

Partonic collectivity is one of the necessary signatures for the formation of Quark-Gluon-Plasma in high-energy nuclear collisions. Number of Constituent Quarks (NCQ) scaling has been observed for light hadron elliptic flow v_2 in top energy nuclear collisions at RHIC and the LHC, and this has been theoretically suggested as strong evidence for partonic collectivity. In this letter, a systematic analysis of v_2 of π^\pm , K^\pm , K_S^0 , p and Λ in Au+Au collisions at $\sqrt{s_{NN}} = 3.2, 3.5, 3.9,$ and 4.5 GeV, with the STAR experiment at RHIC, is presented. NCQ scaling is markedly violated at 3.2 GeV, consistent with a hadronic-interaction dominated equation of state. However, as the collision energy increases, a gradual evolution to NCQ scaling is observed. This beam-energy dependence of v_2 for all hadrons studied provides evidence for the onset of dominant partonic interactions by $\sqrt{s_{NN}} = 4.5$ GeV.

Elliptic flow (v_2), the second-order harmonic coefficient in the Fourier expansion of the final state particle azimuthal distribution with respect to the reaction plane, is sensitive to constituent interactions and the degrees of freedom of the matter created in heavy-ion collisions [1]. The significant v_2 signal and the Number of Constituent Quarks (NCQ) scaling of this elliptic flow are considered as evidence of Quark-Gluon-Plasma (QGP) formation in high-energy relativistic heavy-ion collisions [2–6]. NCQ scaling is understood within the coalescence picture, where hadrons are formed through quark recombination. In this context, light quarks (u, d, s) are mostly thermalized in the medium, leading to a universal pattern of hadron v_2 when scaled by the number of constituent quarks, indicating the presence of quark degrees of freedom in the medium. As the collision energy gradually decreases below a certain threshold, the high temperature and energy density conditions necessary for the formation of QGP will no longer be satisfied. Consequently, the NCQ scaling of elliptic flow is expected to disappear. The Beam Energy Scan (BES) program at the Relativistic Heavy Ion Collider at Brookhaven National Laboratory (RHIC) aims to explore the Quantum Chromodynamics (QCD) phase structure by lowering the collision energy, spanning an energy range from $\sqrt{s_{NN}} = 3$ to 62.4 GeV, in search of possible signals for a QCD first-order phase boundary and a critical point through heavy-ion collision experiments [7–10].

In the elliptic flow measurements of the first phase of RHIC BES, we observed a relatively good agreement of NCQ scaling in collisions with $\sqrt{s_{NN}} \geq 7.7$ GeV [11–14], although observations of a possible deviation from NCQ scaling, around 2σ , were noted for the ϕ meson v_2 in collisions at $\sqrt{s_{NN}} = 7.7$ GeV and 11.5 GeV [11–14]. Further investigation with larger data samples is warranted. The latest published elliptic flow results from the STAR experiment at $\sqrt{s_{NN}} = 3$ GeV show that NCQ scaling breaks among π^+ , K^+ and p at this energy [15].

The second phase of the RHIC BES (BES-II) focuses on energies ranging from $\sqrt{s_{NN}} = 3$ to 19.6 GeV, cor-

responding to a baryon chemical potential range of 750 to 205 MeV [16–18]. To do so, STAR has conducted a series of detector upgrades for BES-II, including: inner Time Projection Chamber (iTPC) to improve the track quality [19]; Event Plane Detector (EPD) to measure the collision centrality and the event plane of the collision event [20]; endcap Time of Flight (eTOF) to enhance the particle identification capability in the mid-rapidity region for the Fixed-Target (FXT) program [21].

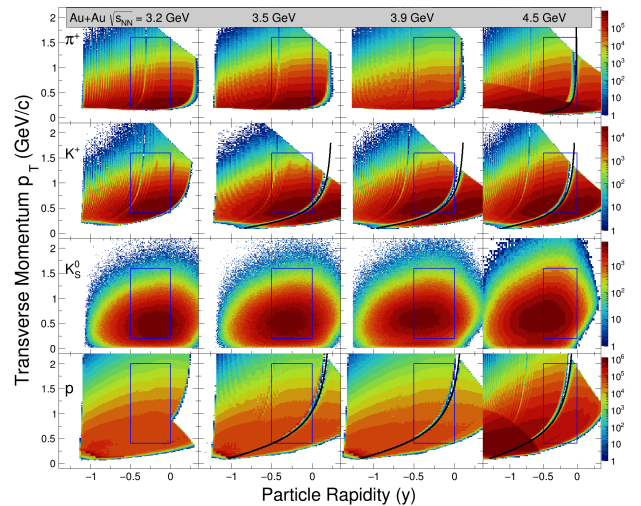


FIG. 1. The transverse momentum (p_T) and identified particle rapidity (y , in the center-of-mass frame) distributions for π^+ , K^+ , K_S^0 , and p from Au+Au collisions at $\sqrt{s_{NN}} = 3.2, 3.5, 3.9,$ and 4.5 GeV. To the right of the black curve is the acceptance provided by eTOF. The blue boxes represent the acceptance ($-0.5 < y < 0$) used for elliptic flow measurements.

In this letter, we report v_2 measurements for π^\pm , K^\pm , K_S^0 , p , and Λ in Au+Au collisions at $\sqrt{s_{NN}} = 3.2, 3.5, 3.9,$ and 4.5 GeV. These data were collected in 2019 and 2020 during the STAR FXT program at RHIC. Datasets for collision energies above 4.5 GeV in the FXT mode are not included due to limited mid-rapidity coverage. The

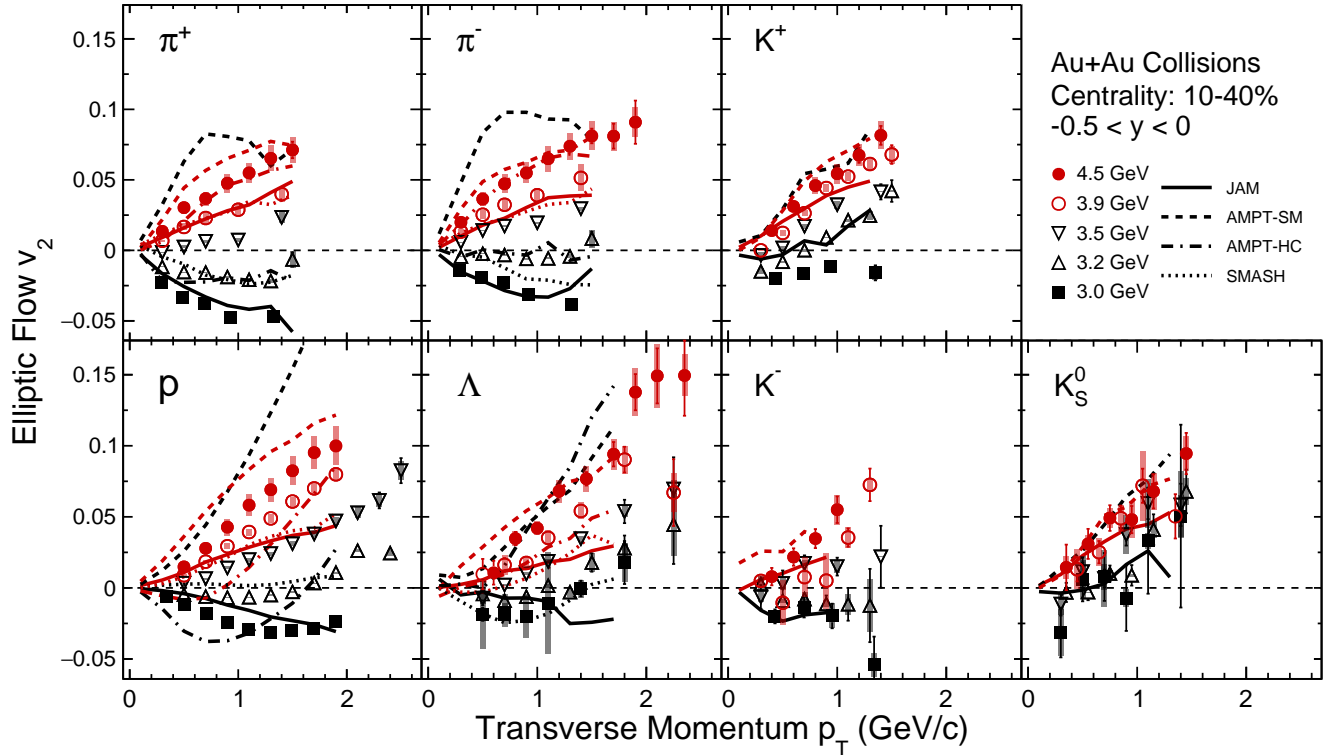


FIG. 2. Transverse momentum (p_T) dependence of v_2 for π^\pm , K^\pm , K_S^0 , p , and Λ in 10-40% centrality for Au+Au collisions at $\sqrt{s_{NN}} = 3.0, 3.2, 3.5, 3.9,$ and 4.5 GeV. Statistical and systematic uncertainties are shown as bars and bands, respectively. Different curves represent the results from JAM (solid), AMPT-SM (dashed), AMPT-HC (dash-dotted), and SMASH (dotted) calculations: red for 4.5 GeV, and black for 3.0 GeV. For clarity, the uncertainties of the model calculations (relative error $\leq 10\%$) are not shown. Calculations of SMASH and AMPT-HC for K^\pm , K_S^0 are omitted, as the results are too similar to JAM to be clearly distinguished. Additionally, the K^- results at 3 GeV are not presented due to the low production yield in the model.

results presented here are analyzed from minimum bias events of Au+Au collisions. The primary vertex position of each event along the beam direction is selected to be within 2 cm from the target, which was located 200 cm from the center of the Time Projection Chamber (TPC). Additionally, the vertex location along the radial direction is chosen to be smaller than 2 cm to eliminate possible beam interactions with the vacuum pipe. Runs where the mean value of physics variables, such as azimuthal angle and pseudo-rapidity, exceeds 5 times the standard deviation across all runs are labeled as bad runs and excluded from the analysis [22]. Pileup events, resulting from the long drift time of TPC electrons relative to the time interval between beam bunches, leading to the misidentification of multiple events as a single event, are removed by correlating the TPC multiplicity with the Time of Flight (TOF) matched multiplicity. Collision centralities are determined by fitting the measured charged particle multiplicities from the TPC with a Monte Carlo Glauber model[23]. To select high-quality tracks, we require a distance of closest approach from the vertex ≤ 3 cm and a minimum of 15 space points within the acceptance of the TPC. For particle identi-

fication (PID) of π^\pm , K^\pm , and p , a combination of the TPC and the TOF detector is used, which relies on the ionization energy loss information and time-of-flight information, respectively. A minimum identification purity of $> 90\%$ is required for elliptic flow measurements, with the PID contamination effect estimated as a systematic uncertainty source. The strange hadrons K_S^0 and Λ are reconstructed by pairing their daughter tracks via the Kalman Filter (KF) particle package [24, 25].

The transverse momentum (p_T) and rapidity (y , in the center-of-mass frame) distributions of identified particles π^+ , K^+ , K_S^0 , and p from Au+Au collisions at $\sqrt{s_{NN}} = 3.2, 3.5, 3.9,$ and 4.5 GeV are shown in Fig. 1. The additional acceptance provided by the eTOF (right side of the black curve) is particularly evident at forward rapidities. The blue boxes show the region ($-0.5 < y < 0$) used to determine the elliptic flow measurements reported in this paper. Due to the asymmetry of the phase space acceptance in fixed-target collisions, the 3-sub event method is applied to reconstruct the event plane and estimate the

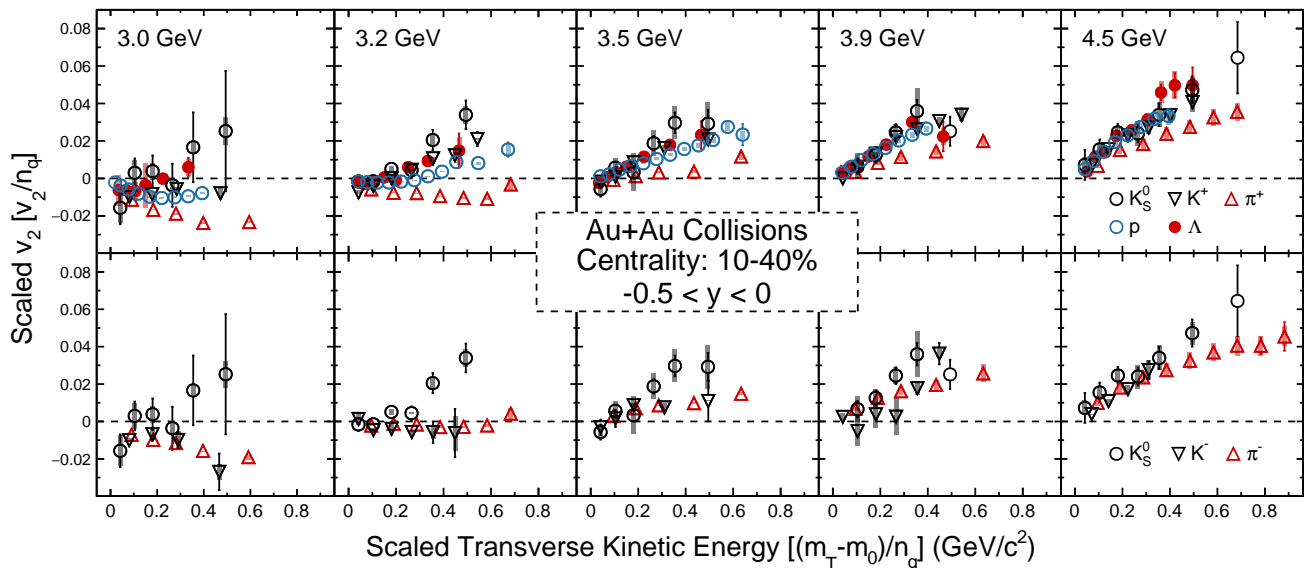


FIG. 3. The number of constituent quarks n_q scaled v_2 as a function of n_q scaled transverse kinetic energy for particles (upper panel) and anti-particles (lower panel) in 10-40% centrality for Au+Au collisions at $\sqrt{s_{NN}} = 3.0, 3.2, 3.5, 3.9,$ and 4.5 GeV. Statistical and systematic uncertainties are shown as bars and bands, respectively.

event plane resolution [26]:

$$\begin{aligned} & \langle \cos [n (\Psi_m^a - \Psi_r)] \rangle \\ &= \sqrt{\frac{\langle \cos [n (\Psi_m^a - \Psi_m^b)] \rangle \langle \cos [n (\Psi_m^a - \Psi_m^c)] \rangle}{\langle \cos [n (\Psi_m^b - \Psi_m^c)] \rangle}}, \end{aligned} \quad (1)$$

where Ψ_r represents the reaction plane, n denotes the corresponding Fourier coefficient v_n , and m indicates the m -th order harmonic event plane. Ψ_m^a , Ψ_m^b , and Ψ_m^c represent the three sub-event planes, determined with pseudo-rapidity (η_{Lab}) ranges of [3.2, 6.1], [2.8, 3.1], and [0, 1.0], respectively, in the laboratory frame. As the first-order coefficient (v_1) is more significant than v_2 within this energy region, v_2 is measured with respect to the first-order event plane, with event plane resolution about 20-40% in mid-central 10-40% collisions.

The p_T dependence of v_2 measurements considers the detector efficiency as a function of transverse momentum p_T and rapidity y . This efficiency encompasses the track reconstruction efficiency of the TPC and the TOF matching efficiency for π^\pm , K^\pm , and p , as well as the additional reconstruction efficiency for K_S^0 and Λ . These efficiencies are estimated using the embedding method within the STAR analysis framework [18, 27–29].

The systematic uncertainties in the measurements are determined by varying the analysis cuts mentioned above, which include track quality cuts, particle identification cuts, and event plane resolution. For each cut variable, we assign the maximum deviation from the default value as the systematic error originating from that source. Assuming these sources are uncorrelated, the total systematic uncertainty is calculated by summing them

together quadratically. A Barlow check [30] was implemented to eliminate the uncertainties introduced by statistical fluctuations during this process. The largest systematic uncertainty in proton v_2 at 4.5 GeV, arising from event plane resolution, is less than 13.3%. The systematic uncertainty from particle identification cuts is less than 1.5%, and less than 1.7% for track quality cuts.

Figure 2 presents the p_T dependence of v_2 for π^\pm , K^\pm , K_S^0 , p , and Λ in 10-40% centrality for Au+Au collisions at $\sqrt{s_{NN}} = 3.0, 3.2, 3.5, 3.9,$ and 4.5 GeV. The data at 3.2, 3.5, 3.9, and 4.5 GeV represent new measurements, while the 3.0 GeV data are taken from a previous publication [15]. Due to the rarity of \bar{p} and $\bar{\Lambda}$ in this collision energy range, measurements of the elliptic flow for these two particles are not available. At lower collision energies, the passing time of projectile and target spectators is comparable to the mean freeze-out time of produced particles [31–33]. As a result, in-plane expansion is hindered by the spectators, leading to negative v_2 values [34, 35]. This effect, known as spectator shadowing, is particularly evident at 3 GeV, where hadrons dominate the medium's degrees of freedom, characterized by large cross sections and short mean-free paths. However, as the collision energy increases, the suppression effect weakens, and v_2 transitions from negative to positive between 3.0 and 4.5 GeV, as shown in Fig. 2. This trend suggests the gradual emergence of partonic degrees of freedom, where interactions are governed by smaller partonic cross sections and longer mean-free paths.

Comparisons with transport models further support this interpretation. The calculations from the Jet AA Microscopic Transport Model (JAM) [36, 37], Multi-Phase

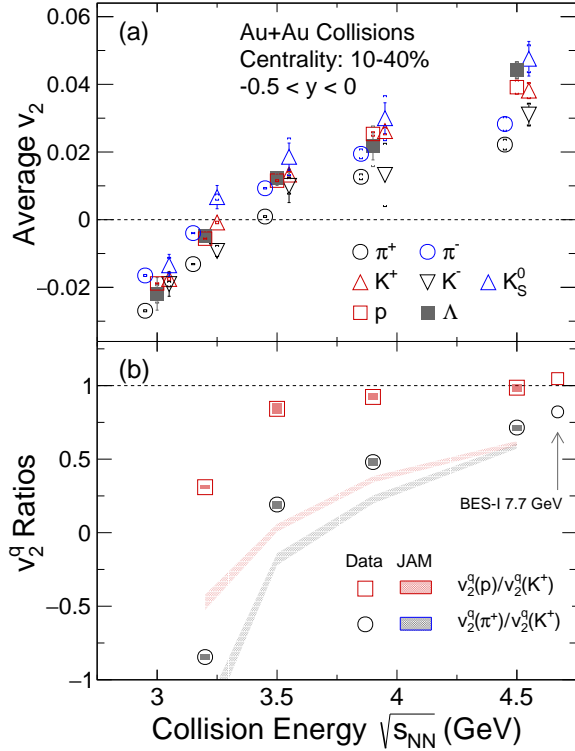


FIG. 4. (a): The energy dependence of p_T integrated v_2 for π^\pm , K^\pm , K_S^0 , p , and Λ in 10-40% centrality from Au+Au collisions at $\sqrt{s_{NN}} = 3.0, 3.2, 3.5, 3.9,$ and 4.5 GeV. For clarity, the x-axis values of pions and kaons are shifted by ± 0.05 respectively. (b): The energy dependence of n_q scaled v_2 ratios of $v_2^q(\pi^+)/v_2^q(K^+)$ and $v_2^q(p)/v_2^q(K^+)$ at $E_T/n_q = 0.4$ GeV/ c^2 in the same centrality. Statistical and systematic uncertainties are shown as bars and bands, respectively. The JAM calculations with baryonic mean field are shown as dashed bands.

Transport Model: Hadron Cascade (AMPT-HC) and String Melting (AMPT-SM) mode [38, 39], and Simulating Many Accelerated Strongly interacting Hadrons (SMASH) [40] are represented by the curves. For the lowest collision energy 3 GeV, the hadronic transport models JAM, AMPT-HC, and SMASH qualitatively describe the v_2 data. The multi-phase transport model AMPT-SM (black dashed curve) predicts the opposite sign of v_2 because it does not account for the finite thickness of the incoming nuclei, thus missing the potential shadowing effect from spectator nucleons. For 4.5 GeV, the hadronic transport models generally underestimate the v_2 data (except π^\pm from AMPT-HC); in contrast, AMPT-SM, which incorporates partonic interactions, better describes the v_2 data. This suggests that parton interactions and the coalescence play an important role in generating such a significant v_2 signal. Detailed comparison of the model calculations can be found in the Supplemental Material.

NCQ scaling is expected to reflect the effective degrees

of freedom of the medium. Figure 3 represents the number of constituent quarks n_q scaled v_2 as a function of n_q scaled transverse kinetic energy E_T ($m_T - m_0$) for particles (upper panel) and anti-particles (lower panel) separately in 10-40% centrality for Au+Au collisions, where $m_T = \sqrt{(p_T^2 + m_0^2)}$. In collisions at 3.0 and 3.2 GeV, it can be clearly observed that the NCQ scaling is broken, with each particle exhibiting a different trend. As the collision energy increases from 3.2 to 4.5 GeV, the NCQ scaling becomes evident. These observations suggest that hadronic interactions dominate the equation of state of the created matter at 3.0 and 3.2 GeV, while partonic interactions become more important at collision energies greater than 3.2 GeV. On the model side, JAM better describes the NCQ breaking at 3.0 GeV but fails to capture the scaling behavior at 4.5 GeV; AMPT-SM shows better scaling behavior than hadronic transport models at 4.5 GeV. Notably, the v_2 of π^\pm is smaller than the scaling of other particles at 4.5 GeV. The p_T/n_q scaling exhibits better performance than $(m_T - m_0)/n_q$ for π^\pm , which is shown in the Supplemental Material, suggesting that the deviation at this energy is primarily attributed to the significantly smaller mass of pions compared to other hadrons.

We further investigate the p_T integrated v_2 as a function of collision energy. Figure 4 (a) shows the energy dependence of p_T integrated v_2 for π^\pm , K^\pm , K_S^0 , p , and Λ in 10-40% centrality from Au+Au collisions at $\sqrt{s_{NN}} = 3.0, 3.2, 3.5, 3.9,$ and 4.5 GeV. The integrated v_2 is calculated within $0.2 < p_T(\text{GeV}/c) < 1.6$ for π^\pm , $0.4 < p_T(\text{GeV}/c) < 1.6$ for K^\pm, K_S^0 , $0.4 < p_T(\text{GeV}/c) < 2.0$ for p, Λ . p_T integrated v_2 changes from negative to positive from 3.0 to 4.5 GeV, crossing zero at about 3.2 GeV. Clear differences between π^- and π^+ are observed at each energy, and the differences become smaller as the energy increases. This is consistent with the picture of the baryon number transport — quarks transported from beam rapidity to mid-rapidity experience more violent scatterings than quarks produced at mid-rapidity [41]. Additionally, the initial nuclear matter is a neutron-rich environment, causing a larger transported effect for $\pi^-(\bar{u}d)$ compared to $\pi^+(u\bar{d})$. Although the uncertainties are large for K^\pm, K_S^0 , these three kaons exhibit ordering behavior, i.e., $K_S^0(d\bar{s}) > K^+(u\bar{s}) > K^-(\bar{u}s)$, which is also consistent with the transported effect. These observations indicate the effect of the transported quarks is also present even at this energy region where the baryon density is high. On the other side, the v_2 of p and Λ are consistent within statistical uncertainties.

In order to quantify the trend of NCQ scaling with collision energy, Fig. 4 (b) shows the n_q scaled v_2 ratios of $v_2^q(\pi^+)/v_2^q(K^+)$ and $v_2^q(p)/v_2^q(K^+)$ at $E_T/n_q = 0.4$ GeV/ c^2 as a function of collision energy, where the v_2^q represents the n_q scaled v_2 (v_2/n_q). The ratio of $v_2^q(p)/v_2^q(K^+)$ is close to unity at 3.9 and 4.5 GeV, while it deviates significantly at 3.2 GeV. Although hadronic

model JAM calculations fit the $v_2(p_T)$ data better at lower collision energies, they underestimate the ratios throughout the energy range studied.

In summary, we present the elliptic flow of identified hadrons π^\pm , K^\pm , K_S^0 , p , and Λ in Au+Au collisions at $\sqrt{s_{NN}} = 3.2, 3.5, 3.9,$ and 4.5 GeV. The v_2 of these particles changes from negative to positive around 3.2 GeV. At the lower colliding energy, $\sqrt{s_{NN}} \leq 3.2$ GeV, NCQ scaling breaks down and the calculations from the hadronic transport model JAM [36, 37] reproduce the transverse momentum dependence of the measured $v_2(p_T)$, implying hadronic interaction dominance. As collision energy increases, a gradual onset of NCQ scaling is observed and the hadronic transport model underpredicts, while the multi-phase transport model more accurately captures the collectivity observed in the 4.5 GeV data. The observed breakdown and subsequent onset of NCQ scaling suggest a dominance of partonic interactions in collisions at $\sqrt{s_{NN}} \geq 4.5$ GeV, signaling the emergence of partonic collectivity.

Acknowledgments: We thank the RHIC Operations Group and SDCC at BNL, the NERSC Center at LBNL, and the Open Science Grid consortium for providing resources and support. This work was supported in part by the Office of Nuclear Physics within the U.S. DOE Office of Science, the U.S. National Science Foundation, National Natural Science Foundation of China, Chinese Academy of Science, the Ministry of Science and Technology of China and the Chinese Ministry of Education, NSTC Taipei, the National Research Foundation of Korea, Czech Science Foundation and Ministry of Education, Youth and Sports of the Czech Republic, Hungarian National Research, Development and Innovation Office, New National Excellency Programme of the Hungarian Ministry of Human Capacities, Department of Atomic Energy and Department of Science and Technology of the Government of India, the National Science Centre and WUT ID-UB of Poland, the Ministry of Science, Education and Sports of the Republic of Croatia, German Bundesministerium für Bildung, Wissenschaft, Forschung und Technologie (BMBF), Helmholtz Association, Ministry of Education, Culture, Sports, Science, and Technology (MEXT), Japan Society for the Promotion of Science (JSPS) and Agencia Nacional de Investigación y Desarrollo (ANID) of Chile.

[1] S. A. Voloshin, A. M. Poskanzer, and R. Snellings, *Landolt-Bornstein* **23**, 293 (2010).
 [2] J. Adams *et al.* (STAR), *Nucl. Phys. A* **757**, 102 (2005).
 [3] K. Adcox *et al.* (PHENIX), *Nucl. Phys. A* **757**, 184 (2005).
 [4] L. Adamczyk *et al.* (STAR), *Phys. Rev. Lett.* **116**, 062301 (2016).
 [5] L. Adamczyk *et al.* (STAR), *Phys. Rev. Lett.* **118**,

212301 (2017).
 [6] P. Braun-Munzinger and J. Stachel, *Nature* **448**, 302 (2007).
 [7] K. Fukushima and T. Hatsuda, *Rept. Prog. Phys.* **74**, 014001 (2011).
 [8] A. Bzdak *et al.*, *Phys. Rept.* **853**, 1 (2020).
 [9] X. Luo, S. Shi, N. Xu, and Y. Zhang, *Particles* **3**, 278 (2020).
 [10] J.-H. Chen *et al.*, *Nuclear Science and Techniques* **35**, 214 (2024).
 [11] L. Adamczyk *et al.* (STAR), *Phys. Rev. Lett.* **110**, 142301 (2013).
 [12] L. Adamczyk *et al.* (STAR), *Phys. Rev. C* **88**, 014902 (2013).
 [13] L. Adamczyk *et al.* (STAR), *Phys. Rev. C* **93**, 014907 (2016).
 [14] L. Adamczyk *et al.* (STAR), *Phys. Rev. C* **86**, 054908 (2012).
 [15] M. S. Abdallah *et al.* (STAR), *Phys. Lett. B* **827**, 137003 (2022).
 [16] J. Cleymans, H. Oeschler, K. Redlich, and S. Wheaton, *Phys. Rev. C* **73**, 034905 (2006).
 [17] A. Andronic, P. Braun-Munzinger, and J. Stachel, *Nucl. Phys. A* **772**, 167 (2006).
 [18] L. Adamczyk *et al.* (STAR), *Phys. Rev. C* **96**, 044904 (2017).
 [19] C. Yang (STAR), *Nucl. Phys. A* **967**, 800 (2017).
 [20] J. Adams *et al.*, *Nucl. Instrum. Meth. A* **968**, 163970 (2020).
 [21] K. Wang *et al.*, *Nucl. Instrum. Meth. A* **1057**, 168778 (2023).
 [22] M. Abdallah *et al.* (STAR), *Phys. Rev. C* **105**, 014901 (2022).
 [23] M. L. Miller, K. Reygers, S. J. Sanders, and P. Steinberg, *Ann. Rev. Nucl. Part. Sci.* **57**, 205 (2007).
 [24] I. Kisel (CBM), *J. Phys. Conf. Ser.* **1070**, 012015 (2018).
 [25] A. Banerjee, I. Kisel, and M. Zyzak, *Int. J. Mod. Phys. A* **35**, 2043003 (2020).
 [26] A. M. Poskanzer and S. A. Voloshin, *Phys. Rev. C* **58**, 1671 (1998).
 [27] B. I. Abelev *et al.* (STAR), *Phys. Rev. C* **79**, 034909 (2009).
 [28] M. M. Aggarwal *et al.* (STAR), *Phys. Rev. C* **83**, 024901 (2011), [Erratum: *Phys.Rev.C* 107, 049903 (2023)].
 [29] M. Abdallah *et al.* (STAR), *Phys. Rev. C* **104**, 024902 (2021), [Erratum: *Phys.Rev.C* 111, 029902 (2025)].
 [30] R. Barlow, in *Conference on Advanced Statistical Techniques in Particle Physics* (2002) pp. 134–144, arXiv:hep-ex/0207026.
 [31] H. Liu, S. Panitkin, and N. Xu, *Phys. Rev. C* **59**, 348 (1999).
 [32] A. Le Fèvre, Y. Leifels, C. Hartnack, and J. Aichelin, *Phys. Rev. C* **98**, 034901 (2018).
 [33] Z.-W. Liu and S. Shi, *Phys. Rev. C* **110**, 034903 (2024).
 [34] J. Adamczewski-Musch *et al.* (HADES), *Phys. Rev. Lett.* **125**, 262301 (2020).
 [35] J. Adamczewski-Musch *et al.* (HADES), *Eur. Phys. J. A* **59**, 80 (2023).
 [36] Y. Nara and A. Ohnishi, *Phys. Rev. C* **105**, 014911 (2022).
 [37] Y. Nara, A. Jinno, K. Murase, and A. Ohnishi, *Phys. Rev. C* **106**, 044902 (2022).
 [38] Z.-W. Lin *et al.*, *Phys. Rev. C* **72**, 064901 (2005).
 [39] G.-C. Yong, *Phys. Lett. B* **848**, 138327 (2024).

- [40] J. Weil *et al.* (SMASH), Phys. Rev. C **94**, 054905 (2016). [41] J. C. Dunlop, M. A. Lisa, and P. Sorensen, Phys. Rev. C **84**, 044914 (2011).

Supplemental Material: Observation of the Onset of Constituent Quark Number Scaling in Heavy-Ion Collisions at RHIC

The STAR Collaboration

(Dated: April 4, 2025)

DATA-MODEL COMPARISON: p_T DEPENDENCE OF v_2

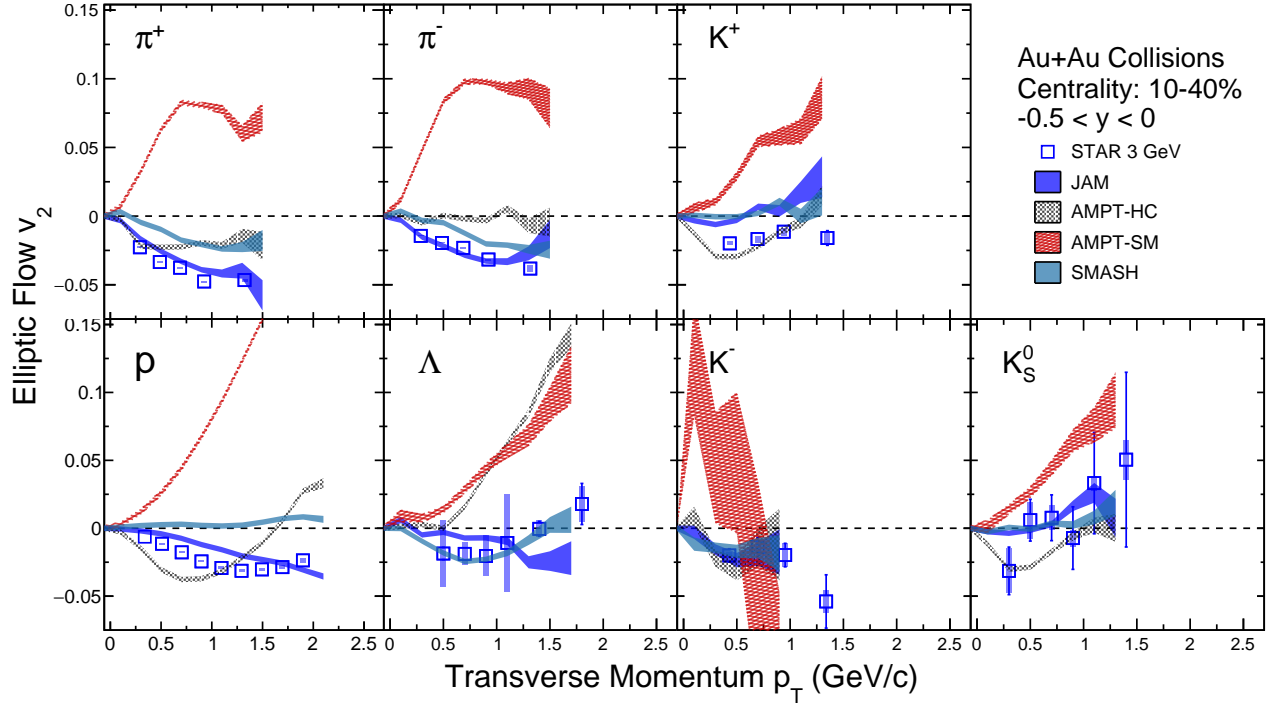


FIG. 1. Transverse momentum (p_T) dependence of v_2 for π^\pm , K^\pm , K_S^0 , p , and Λ in 10-40% centrality for Au+Au collisions at $\sqrt{s_{NN}} = 3.0$ GeV. Statistical and systematic uncertainties are shown as bars and bands, respectively. Different bands represent the results from JAM (blue), AMPT-HC (black), AMPT-SM (red), and SMASH (cyan) calculations.

Figure 1 presents the p_T dependence of π^\pm , K^\pm , K_S^0 , p , and Λ in 10-40% centrality for Au+Au collisions at $\sqrt{s_{NN}} = 3.0$ GeV. Calculations from different models are represented by the bands, where the “JAM” means Jet AA Microscopic Transport Model [1, 2] with soft Equation Of State (EOS); “AMPT-HC” and “AMPT-SM” refer to Hadron Cascade and String Melting mode of the Multi-Phase Transport Model [3, 4]; “SMASH” means Simulating Many Accelerated Strongly interacting Hadrons [5] with soft EOS. The hadronic transport models JAM, AMPT-HC, and SMASH qualitatively describe the v_2 data, while the multi-phase transport model AMPT-SM (red band) predicts the opposite sign of v_2 , because it does not account for the finite thickness of the incoming nuclei, thus missing the potential shadowing effect from spectator nucleons.

Figure 2 shows the p_T dependence of π^\pm , K^\pm , K_S^0 , p , and Λ in 10-40% centrality for Au+Au collisions at $\sqrt{s_{NN}} = 4.5$ GeV. The hadronic transport models generally underestimate the v_2 data (except π^\pm from AMPT-HC); in contrast, AMPT string melting mode better describes the v_2 data.

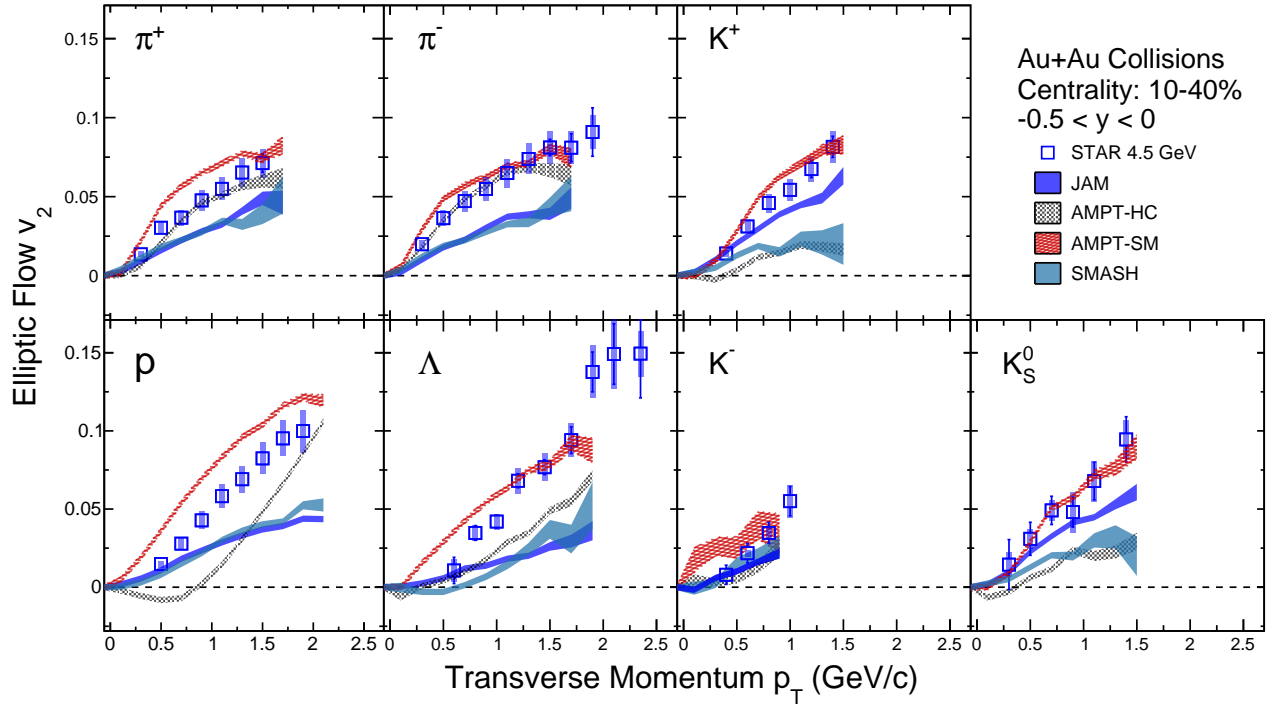


FIG. 2. Transverse momentum (p_T) dependence of v_2 for π^\pm , K^\pm , K_S^0 , p , and Λ in 10-40% centrality for Au+Au collisions at $\sqrt{s_{NN}} = 4.5$ GeV. Statistical and systematic uncertainties are shown as bars and bands, respectively. Different bands represent the results from JAM (blue), AMPT-HC (black), AMPT-SM (red), and SMASH (cyan) calculations.

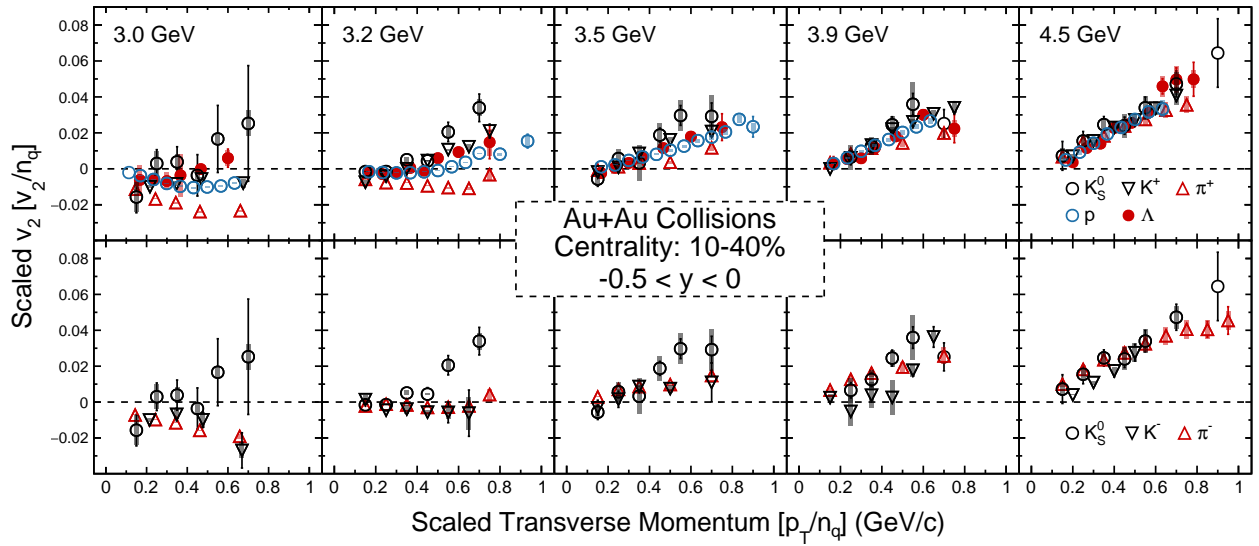


FIG. 3. The number of constituent quarks n_q scaled v_2 as a function of n_q scaled transverse momentum for particles (upper panel) and anti-particles (lower panel) in 10-40% centrality for Au+Au collisions at $\sqrt{s_{NN}} = 3.0, 3.2, 3.5, 3.9,$ and 4.5 GeV.

NUMBER OF CONSTITUENT QUARKS SCALING: v_2/n_q VS. p_T/n_q

Figure 3 represents the number of constituent quarks n_q scaled v_2 as a function of n_q scaled p_T for particles and anti-particles separately in 10-40% centrality for Au+Au collisions. The p_T/n_q scaling exhibits better performance than $(m_T - m_0)/n_q$ scaling for π^\pm , suggesting that the π^\pm deviation on $(m_T - m_0)/n_q$ scaling at 4.5 GeV, may

primarily be attributed to the significantly smaller mass of pions compared to other hadrons.

-
- [1] Y. Nara and A. Ohnishi, Phys. Rev. C **105**, 014911 (2022).
 - [2] Y. Nara, A. Jinno, K. Murase, and A. Ohnishi, Phys. Rev. C **106**, 044902 (2022).
 - [3] Z.-W. Lin *et al.*, Phys. Rev. C **72**, 064901 (2005).
 - [4] G.-C. Yong, Phys. Lett. B **848**, 138327 (2024).
 - [5] J. Weil *et al.* (SMASH), Phys. Rev. C **94**, 054905 (2016).